

Evaluation of numerical strategies for LES of two-phase reacting flows

By E. Riber^{*,†}, M. García^{*}, V. Moureau⁺, H. Pitsch⁺, O. Simonin[†]
and T. Poinsot[†]

Predicting particle dispersion in recirculating two-phase flows is a key issue for reacting flows. In this study, Euler/Euler and Euler/Lagrange LES formulations have been compared in the bluff-body configuration from Borée *et al.* (2001) where glass beads are injected into a complex recirculating flow. These tests are performed for non-reacting, non-evaporating sprays but are mandatory validations before computing realistic combustion chambers. Two different solvers (one explicit and compressible and the other implicit and incompressible) have also been tested on the same configuration. Results show that the gas flow is well predicted by both solvers. The dispersed phase is also well predicted but the Lagrange solver predicts RMS values more precisely. The importance of inlet boundary conditions for the gas and the dispersed phase is revealed through various tests.

1. Motivations and objectives

Today, RANS (Reynolds-averaged Navier-Stokes) equations are routinely solved to design combustion chambers, for both gaseous and liquid fuels. Recently, in order to provide better accuracy for the prediction of mean flows but also to give access to unsteady phenomena occurring in combustion devices (such as instabilities, flashback or quenching), Large-Eddy Simulation (LES) has been extended to reacting flows. The success of these approaches for gaseous flames in the last years (Caraeni *et al.* 2000; Chakravarthy & Menon 2000; Colin *et al.* 2000; Forkel & Janicka 2000; Pitsch & Duchamp de la Geneste 2002; Mahesh *et al.* 2004; Selle *et al.* 2004; Sommerer *et al.* 2004; Moureau *et al.* 2005; Roux *et al.* 2005; Poinsot & Veynante 2005) is a clear illustration of their potential. LES gives access to the large scales structures of the flow reducing the importance of modeling, and naturally capturing a significant part of the physics controlling these flames. Even though LES has already demonstrated its potential for gaseous flames, its extension to two-phase flames is still largely to be done. First, the physical submodels required to describe the atomization of a liquid fuel jet, the dispersion of solid particles, their interaction with walls, evaporation and combustion are as difficult to build in LES as in RANS because they are essentially subgrid phenomena. Second, the numerical implementation of two-phase flow LES remains a challenge. The equations for both the gaseous and the dispersed phases must be solved together at each time step in a strongly coupled manner. This differs from classical RANS where the resolution of the two phases can be done in a weak procedure, bringing first the gas flow to convergence, then the solid particles and finally iterating until convergence of both phases. Finally, in

[†] IMF Toulouse, UMR CNRS/INPT/UPS, 31400 Toulouse, France

^{*} CERFACS, CFD team, 42 Av. Gaspard Coriolis, 31057 Toulouse, France

⁺ Center for Turbulence Research

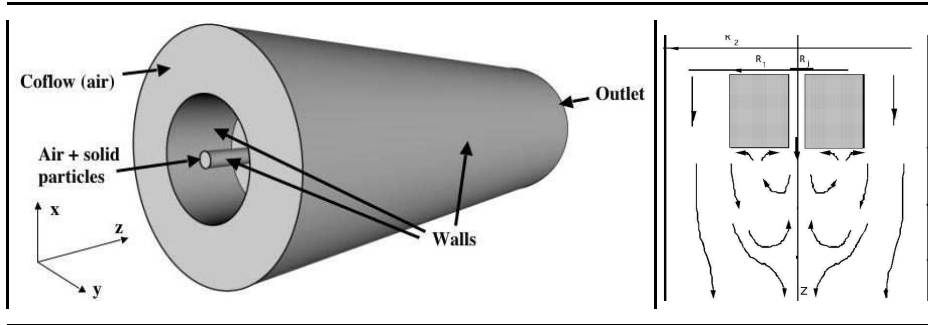


FIGURE 1. Configuration of Borée (Borée *et al.* 2001). The dimensions are : $R_j = 10$ mm, $R_1 = 75$ mm, $R_2 = 150$ mm. The total length of the experiment is 1.5 m.

the context of parallel super-computing, numerical efficiency is an additional constraint. For single-phase flows, efficient and accurate solvers have been developed and speedups of the order of 5000 are not uncommon (www.cerfacs.fr/cfd/parallel.html). Maintaining a similar parallel efficiency for a two-phase flow solver while representing the main physics of the flow raises additional questions.

In LES of two-phase flows, physics and numerics interact strongly: the first question is to choose a paradigm to describe the two-phase flow. Most RANS codes use Euler/Lagrange (EL) methods in which the flow is solved using an Eulerian method and the particles are tracked using a Lagrangian approach. An alternative technique is to use two-fluid models in which both the gas and the dispersed phases are solved using an Eulerian method (Euler/Euler or EE). The history of RANS development has shown that both EE and EL are useful and either is found today in most commercial codes. For LES, both EE and EL formulations are being developed and the focus of this study is to test them in a reference case where complete sets of solutions for gas and dispersed phase are available. This exercise is performed here without evaporation or combustion.

2. Configuration and work objectives

In this study two solvers developed at CTR and CERFACS are used to investigate some critical issues for LES of two-phase flows on massively parallel computers:

- an implicit incompressible solver (CDP) using a EL formulation. For this study, hexahedron-based grids are used in CDP.

- an explicit compressible solver (AVBP) using both EL and EE formulations (Kaufmann *et al.* 2003). For the present study, AVBP is used on tetrahedron-based grids.

These solvers are used to study a bluff-body configuration (Borée *et al.* 2001) where a jet of air and solid particles are injected in a coflow of air (Fig. 1). The jet velocity on the axis is 4 m/s and the coflow maximum velocity is 6 m/s. The experiment is designed to provide large recirculation zones between the central jet and the coflow. The dispersed phase consists of solid particles (glass beads with diameter ranging from 20 to 100 microns with a mean value of 60 microns) so that evaporation, coalescence and break up do not have to be considered. The material density of the glass particle is $\rho_p = 2470$ kg.m⁻³. The mass loading ratio of particles in the inner jet is 0.22 corresponding to a solid volumetric fraction less than 10^{-4} . Thus collision effects will be assumed to be

negligible in the modelling approaches.

The issues which can be studied are still very relevant for LES of two-phase flows:

- Compare performances and cost of EE and EL approaches.
- Evaluate influence of mesh type (hexahedra vs tetrahedra).
- Compare implicit and explicit formulations for time advancement.
- Study effects of boundary conditions for the dispersed phase: should the particle velocities at the domain inlet be modulated to account for turbulence or not?

3. Description of solvers and models

Numerical methods used in both LES solvers for the gas phase have been extensively described in the literature (Moureau *et al.* 2005; Selle *et al.* 2004; Schmitt *et al.* 2006; Mahesh *et al.* 2004; Ham & Iaccarino 2004) and will only be summarized here.

The LES solver CDP solves implicitly the incompressible Navier-Stokes equations. The time integration of CDP is based on the fractional-step method (Kim & Moin 1985) and the space integration relies on a second-order central scheme which conserves the kinetic energy (Mahesh *et al.* 2004; Ham & Iaccarino 2004). The dynamic Smagorinsky model (Germano *et al.* 1991) is used to model the subgrid stress tensor.

The explicit LES solver AVBP solves the compressible Navier-Stokes equations with a third-order scheme for spatial differencing and a Runge-Kutta time advancement (Colin & Rudgyard 2000; Moureau *et al.* 2005). For the present case, the Smagorinsky model is used to model SGS tensors. Walls are treated using the law-of-the-wall formulation of Schmitt *et al.* (2006). The boundary conditions are handled with the NSCBC formulation (Poinsot & Veynante 2005; Moureau *et al.* 2005).

The influence of the particles on the gas phase is taken into account in the EL simulations by using the point-force approximation in the general framework of the particle-in-cell method (PIC) (Boivin *et al.* 1998; Vermorel *et al.* 2003), with standard single-phase subgrid turbulence modelling approaches. According to Boivin *et al.* (2000), such an assumption is valid for small mass loading ratio of particles (typically, $\alpha_p \rho_p / \rho_g \leq 1$) with response time larger than the subgrid turbulence characteristic time scale.

The influence of the particles on the gas phase is taken into account through the drag force in the EE simulations. Modification of the gas subgrid-scale turbulence model by the particles is neglected.

This section focuses on techniques used for the dispersed phase.

Euler/Lagrange approach

The dispersed phase consists of particles which are assumed to be rigid spheres with diameter comparable or smaller than the Kolmogorov length scale. If the particle density is much larger than the fluid density, the forces acting on particles reduce to drag and gravity. With these assumptions, the particle equations of motion can then be written for a single particle as:

$$\frac{dx_{p,i}}{dt} = u_{p,i} \quad (3.1)$$

$$\frac{du_{p,i}}{dt} = -\frac{3}{4} \frac{\rho_g}{\rho_p} \frac{C_D}{d_p} |\mathbf{v}_r| v_{r,i} + g_i = -\frac{u_{p,i} - \tilde{u}_{g,i}}{\tau_p} + g_i \quad (3.2)$$

The local drag coefficient in Eq. (3.2) is C_D and may be expressed in terms of the particle Reynolds number Re_p following Schiller & Nauman (1935):

$$C_D = \frac{24}{Re_p} [1 + 0.15Re_p^{0.687}], \quad Re_p = \frac{|\mathbf{v}_r| d_p}{\nu_g} \leq 800. \quad (3.3)$$

The local instantaneous relative velocity between the particle and the surrounding fluid is $\mathbf{v}_{r,i} = u_{p,i} - \tilde{u}_{g,i}$ where g_i is the gravity vector and $\tilde{u}_{g,i}$ is the filtered fluid velocity at the position of the particle assuming that the flow field is locally undisturbed by the presence of this particle (Gatignol 1983; Maxey & Riley 1983) and that the subgrid fluid velocity seen by the particles is negligible (Fede *et al.* 2006). The particle relaxation time τ_p is defined as the Stokes characteristic time:

$$\tau_p = \frac{4}{3} \frac{\rho_p}{\rho_g} \frac{d_p}{C_D} |\mathbf{v}_r| \quad (3.4)$$

where d_p is the particle diameter, ρ_p is the density of the particle, ν_g is the kinematic viscosity of the fluid at the particle location.

Euler/Euler approach

The treatment of the dispersed phase is based on an Eulerian approach: Eulerian equations for the dispersed phase may be derived by several means. A popular and simple way consists in volume filtering of the separate, local, instantaneous phase equations accounting for the inter-facial jump conditions (Druzhinin & Elghobashi 1999). Such an averaging approach is restrictive because particle sizes and particle distances have to be smaller than the smallest length scale of the turbulence. Besides, they do not account for the Random Uncorrelated Motion (Février *et al.* 2005). In the present study, a statistical approach analogous to kinetic theory (Chapman & Cowling 1939) is used to construct a probability density function (pdf) $\check{f}_p(\mathbf{c}_p, \mathbf{x}, t)$ which gives the local instantaneous probable number of particles with the given translation velocity $\mathbf{u}_p = \mathbf{c}_p$. The resulting model (Février *et al.* 2005; Moreau *et al.* 2005) leads to equations for the particle number density \bar{n}_p and the correlated velocity $\hat{\mathbf{u}}_p$:

$$\frac{\partial}{\partial t} \bar{n}_p + \frac{\partial}{\partial x_j} \bar{n}_p \hat{u}_{p,j} = 0 \quad (3.5)$$

$$\begin{aligned} \frac{\partial}{\partial t} \bar{n}_p \hat{u}_{p,i} + \frac{\partial}{\partial x_j} \bar{n}_p \hat{u}_{p,i} \hat{u}_{p,j} &= -\frac{\bar{n}_p}{\tau_p} (\hat{u}_{p,i} - \hat{u}_{f,i}) + \bar{n}_p g_i - \frac{\partial}{\partial x_j} T_{p,ij} \\ &- \frac{\partial}{\partial x_j} \bar{n}_p \widehat{\delta R}_{p,ij}^* - \frac{\partial}{\partial x_i} \frac{2}{3} \bar{n}_p \widehat{\delta \theta}_p \end{aligned} \quad (3.6)$$

where \bar{n}_p , $\hat{\mathbf{u}}_p$ and $\widehat{\delta \theta}_p$ are respectively the filtered particle number density, correlated velocity and Random Uncorrelated Energy (RUE). The two first terms of the rhs of Eq. (3.6) are the drag force and gravity effects on large scales, the third one accounts for the SGS effects, the fourth one takes into account the RUE effects and the last one is a dissipation term by RUE. $T_{p,ij}$ stands for the particle subgrid stress tensor:

$$T_{p,ij} = \bar{n}_p (u_{p,i} \widehat{u}_{p,j} - \hat{u}_{p,i} \hat{u}_{p,j}) \quad (3.7)$$

As in fluid anisotherm turbulence, an additional equation on energy is needed. The transport equation of filtered RUE is:

$$\begin{aligned} \frac{\partial}{\partial t} \bar{n}_p \widehat{\delta\theta}_p + \frac{\partial}{\partial x_j} \bar{n}_p \hat{u}_{p,j} \widehat{\delta\theta}_p = & -2 \frac{\bar{n}_p}{\tau_p} \widehat{\delta\theta}_p - \frac{2}{3} \bar{n}_p \widehat{\delta\theta}_p \frac{\partial \hat{u}_{p,j}}{\partial x_j} \\ & - \bar{n}_p \widehat{\delta R}_{p,ij}^* \frac{\partial \hat{u}_{p,i}}{\partial x_j} - \frac{1}{2} \frac{\partial}{\partial x_j} \bar{n}_p \widehat{\delta S}_{p,ij} + \Pi_{\delta\theta_p} - \frac{\partial}{\partial x_j} Q_{p,j} \end{aligned} \quad (3.8)$$

The first rhs term is the RUE destruction by drag force, the second one is a RUE-dilatation term, the third one is a production term by filtered Random Uncorrelated Velocity (RUV) tensor, the next one is the diffusion by filtered RUV third correlation tensor. $\Pi_{\delta\theta_p}$ and $Q_{p,j}$ are respectively production and diffusion terms by subgrid scales:

$$\Pi_{\delta\theta_p} = \left(\overline{\check{n}_p \delta R_{p,ij} \frac{\partial \hat{u}_{p,i}}{\partial x_j}} - \bar{n}_p \widehat{\delta R}_{p,ij} \frac{\partial \hat{u}_{p,i}}{\partial x_j} \right) \quad \text{and} \quad Q_{p,i} = \bar{n}_p \left(\widehat{u_{p,i} \delta\theta_p} - \hat{u}_{p,i} \widehat{\delta\theta}_p \right) \quad (3.9)$$

Closure of filtered RUV terms

Using an equilibrium assumption, Kaufmann (2004) model $\delta R_{p,ij}^*$ by a viscous term and $\delta S_{p,ij}$ by a diffusive term similar to Fick's law. For LES approach these models are adapted by replacing non filtered quantities by filtered ones leading to (Moreau *et al.* 2005):

$$\widehat{\delta R}_{p,ij}^* = -\hat{\nu}_{RUM} \left(\frac{\partial \hat{u}_{p,i}}{\partial x_j} + \frac{\partial \hat{u}_{p,j}}{\partial x_i} - \frac{\partial \hat{u}_{p,k}}{\partial x_k} \frac{\delta_{ij}}{3} \right) \quad \text{and} \quad \frac{1}{2} \widehat{\delta S}_{p,ij} = -\hat{\kappa}_{RUM} \frac{\partial \widehat{\delta\theta}_p}{\partial x_j} \quad (3.10)$$

where the RUM viscosity, $\hat{\nu}_{RUM}$, and the RUM diffusion coefficient, $\hat{\kappa}_{RUM}$, are given by:

$$\hat{\nu}_{RUM} = \frac{\tau_p}{3} \widehat{\delta\theta}_p \quad \text{and} \quad \hat{\kappa}_{RUM} = \frac{10}{27} \tau_p \widehat{\delta\theta}_p \quad (3.11)$$

Subgrid terms modeling

By analogy to single phase flows (Moin *et al.* 1991; Vreman *et al.* 1995), Riber *et al.* (2005) propose a viscosity model for the SGS tensor $T_{p,ij}$. The trace-free SGS tensor is modeled using a viscosity assumption (compressible Smagorinsky model), while the subgrid energy is parametrized by a Yoshizawa model (Yoshizawa 1986):

$$T_{p,ij} = -C_S 2 \Delta_f^2 \bar{n}_p |\hat{S}_p| (\hat{S}_{p,ij} - \frac{\delta_{ij}}{3} \hat{S}_{p,kk}) + C_I 2 \Delta_f^2 \bar{n}_p |\hat{S}_p|^2 \delta_{ij} \quad (3.12)$$

where \hat{S}_p is the filtered particle strain rate tensor, $|\hat{S}_p|^2 = 2 S_{p,ij} S_{p,ij}$ and Δ_f the filter characteristic length. The model constants have been evaluated in a priori tests (Riber *et al.* 2006) leading to the values $C_S = 0.02$, $C_I = 0.012$.

The subgrid diffusion term in the filtered RUE is modeled by an eddy-diffusivity model:

$$Q_{p,j} = - \frac{\bar{n}_p C_S 2 \Delta_f^2 |\hat{S}_p| \partial \widehat{\delta\theta}_p}{P_{r,p}^{SGS} \partial x_j} \quad (3.13)$$

with the particle turbulent Prandtl number $P_{r,p}^{SGS} = 0.8$. The subgrid production of filtered RUE term $\Pi_{\delta\theta_p}$ acts like a dissipation term in the subgrid energy equation. Using an equilibrium assumption on the particle correlated subgrid energy and neglecting

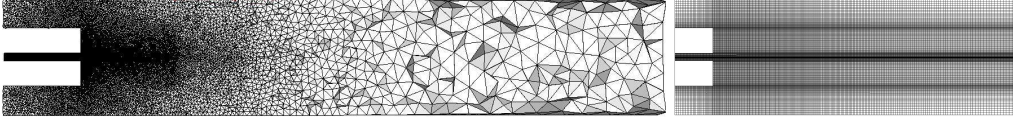


FIGURE 2. Grids used by AVBP (Tetrahedra, left) and CDP (Hexahedra, right).

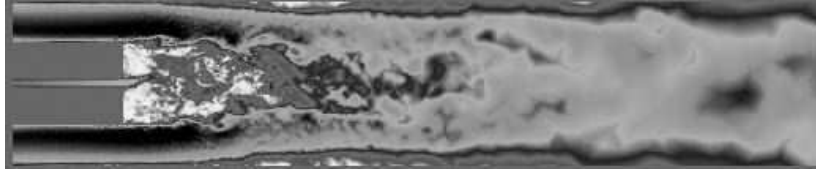


FIGURE 3. Instantaneous field of velocity modulus (AVBP). Maximum value (black): 6 m/s. Minimum value: 0.

	CDP	AVBP
Grid type	Hexahedra	Tetrahedra
Number of cells / nodes	3207960 / 3437576	2058883 / 367313
Time step (microseconds) / CFL	147 / 50	3, 2 / 0.7
Averaging time (s) / Iterations	2, 65 / 18000	1, 03 / 320000
LES model / Wall model	Dynamic Smagorinsky/None	Smagorinsky/Law-of-the-wall

TABLE 1. Summary of parameters and models used for the 'no-particles' computation.

diffusion terms leads to:

$$-\frac{\bar{n}_p}{\tau_p} \left(\frac{T_{p,kk}}{\bar{n}_p} - q_{fp,SGS} \right) + \Pi_{\delta\theta_p} - T_{p,ij} \frac{\partial \hat{u}_{p,i}}{\partial x_j} = 0 \quad (3.14)$$

where the subgrid covariance is $q_{fp,SGS} = u_{p,k} \widehat{u_{f,k}} - \hat{u}_{p,k} \hat{u}_{f,k}$. To first order, the drag force term can be neglected and $\Pi_{\delta\theta_p}$ can be modeled by: $\Pi_{\delta\theta_p} \approx T_{p,ij} \partial \hat{u}_{p,i} / \partial x_j$ with the SGS tensor modeled by Eq. (3.12). This model ensures that the correlated energy dissipated by subgrid effects is fully transferred into RUE.

4. Comparison of gas flow without particles

Before discussing results for the dispersed phase, the accuracy of the LES solvers for the gas phase is evaluated by computing the flow without particles and comparing it to the same data provided in Borée *et al.* (2001). The two codes (AVBP and CDP) are used on two different grids (Fig. 2) (see summary in Table 1). A typical snapshot of the velocity field (modulus) in the central plane is displayed in Fig. 3 for an AVBP result (CDP fields are very similar). The complex structure of the recirculating flow is obvious: on the axis, the flow is recirculating down to $z = 200$ mm. On the sides of the channel, the flow also seems to separate from $z = 50$ mm to $z = 400$ mm.

Figures 4 to 7 present the results of the two LES codes along with the experimental

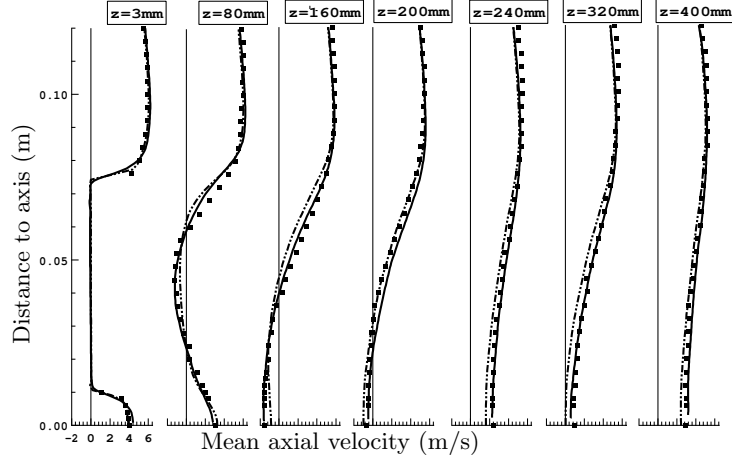


FIGURE 4. Radial profiles of mean axial gas velocities at 7 stations along z axis. Symbols: experiment; solid line: AVBP; dot-dashed line: CDP.

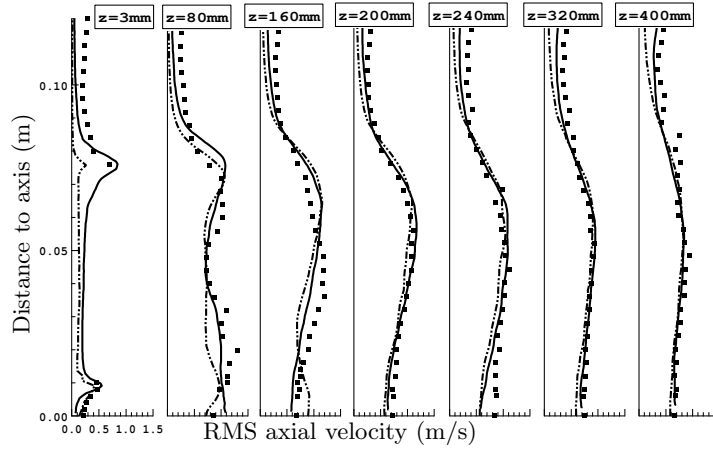


FIGURE 5. Radial profiles of RMS axial gas velocities at 7 stations along z axis. Symbols: experiment; solid line: AVBP; dot-dashed line: CDP.

measurements. The two LES solvers capture most of the flow physics: the axial mean and RMS velocities (Fig. 4 and 5) agree with the LDV measurements. The length of the recirculation zone (evidenced by the negative values of axial velocities on the axis) is well predicted. In the coflow, the RMS values predicted by LES are too low because no turbulence is injected at the inlet of the domain for these computations.

The mean radial velocity levels (Fig. 6) remain small (less than 1 m/s) and the two LES codes capture the radial velocity fields correctly except at the corner of the coflow and the step (first station at $z = 3$ mm) where the RMS velocities are underpredicted by CDP (Fig. 7). The stagnation point (around $z = 170$ mm) is a delicate zone where both codes have difficulties. The source of this problem is the exact position of the stagnation point: any small mismatch in this position leads to large changes in profiles measured around this point. Upstream and downstream of this point, the agreement is very good.

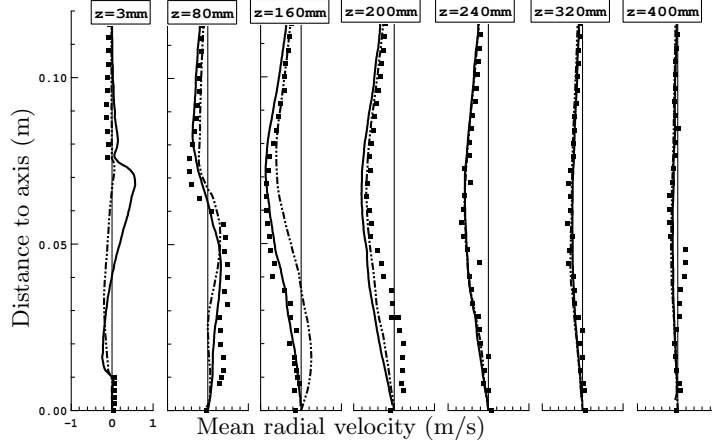


FIGURE 6. Radial profiles of mean radial gas velocities at 7 stations along z axis. Symbols: experiment; solid line: AVBP; dot-dashed line: CDP.

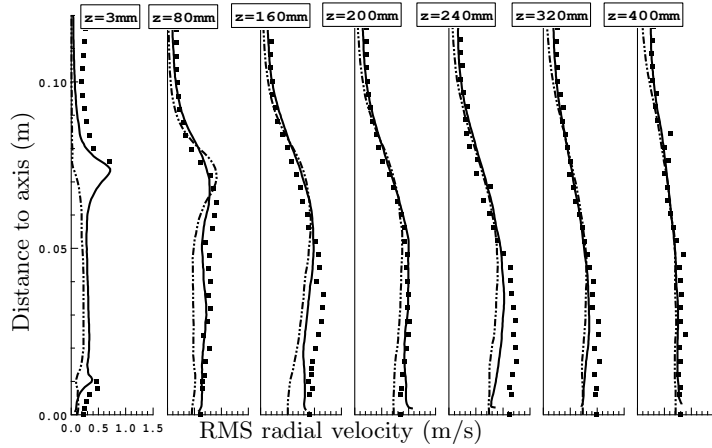


FIGURE 7. Radial profiles of RMS radial gas velocities at 7 stations along z axis. Symbols: experiment; solid line: AVBP; dot-dashed line: CDP.

The overall result is that both codes provide similar results even though they use totally different grids and methods. This indicates that grid independency for the gas is achieved for this test case and that tests for the dispersed phase can be performed with reasonable confidence.

5. Results for two-phase flow cases

This section presents results for the 22 percent mass loading of the central jet, obtained with three different computations summarized in Table 2. The grids and the time steps used in AVBP and CDP are the same as in Table 1[†]. In all computations presented here, the injected particles have a size of 60 microns. Separated studies which are not reported

[†] For these runs, the RUM model is not used and the $\widehat{\delta\theta}_p$ term in Eq. (3.6) is set to zero.

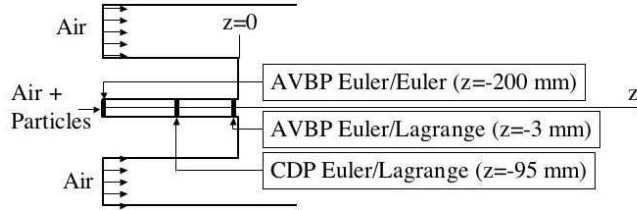


FIGURE 8. Injection position for particles.

	CDP Euler/Lagrange	AVBP Euler/Lagrange	AVBP Euler/Euler
Averaging time (s)	4	0.43	0.64
Particle mean speed	Exp. profile	Exp. profile	Exp. profile
Turbulent fluctuations	White noise (10 %)	White noise (12 %)	Zero
Particle distribution	Homogeneous	Homogeneous	Exp. profile

TABLE 2. Summary of parameters and models used for the particle injection (22 percent mass loading computation). The particles are injected in the central tube.

here, using the Lagrangian solver and multidisperse particles or 60 microns particles only have shown that using a monodisperse distribution of size was very close to the 22 percent case of Borée *et al.* (2001) and was sufficient to capture both the mean flow effects on the gas (through two-way coupling) and the dynamics of the 60 microns class.

An essential part of these LES is the introduction of the particles in terms of position and velocity (Fig. 8). The injection planes are not the same for all codes. The methodologies used to inject the particles are also different to evaluate their impact on results. In AVBP-EE, both the mass loading and the mean velocity imposed in the injection plane ($z = -200$ mm) are the ones measured experimentally at $z = 3$ mm. No turbulent fluctuations are introduced. In AVBP-EL and in CDP, the mass loading is homogeneous over the injection section and the injection speed profile is also the experimental one measured at $z = 3$ mm. In AVBP-EL and in CDP, a white noise (amplitude of the order of 10 percent of the mean velocity) is added to the particle mean velocity profiles to match experimental measurements at $z = 3$ mm.

The velocity fields for the gas phase change when the particles are injected but these effects are limited and are not discussed here. Figures 9 to 12 show velocity fields for particles obtained with the three codes along with the measurements of Borée. The agreement between the experiments and the three LES sets of data is good. An interesting result is that AVBP-EL (dashed line) and AVBP-EE (solid line) provide extremely similar results showing that the EE approach is able to compute such a flow and to provide results which are equivalent in precision to an EL computation.

The best results are obtained with CDP and injection of turbulence on the gas phase. A convenient way to look at the results is to consider the central z axis of the configuration: a critical zone is located around $z = 160$ mm where the stagnation point for the gas is. This is also a zone where particles accumulate and must stop before turning around to escape from the recirculating flows by the sides. Figure 13 shows fields of gas velocity and

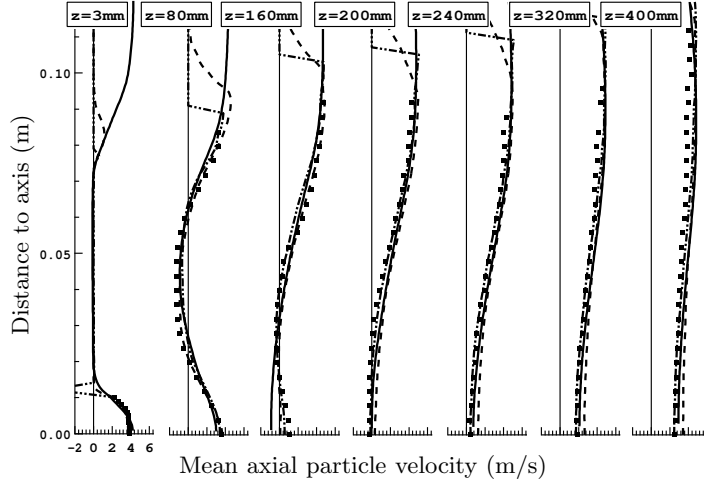


FIGURE 9. Radial profiles of mean axial particle velocities at 7 stations along z axis. Symbols: experiment; solid line: AVBP-EE; dashed line: AVBP-EL; dot-dashed line: CDP.

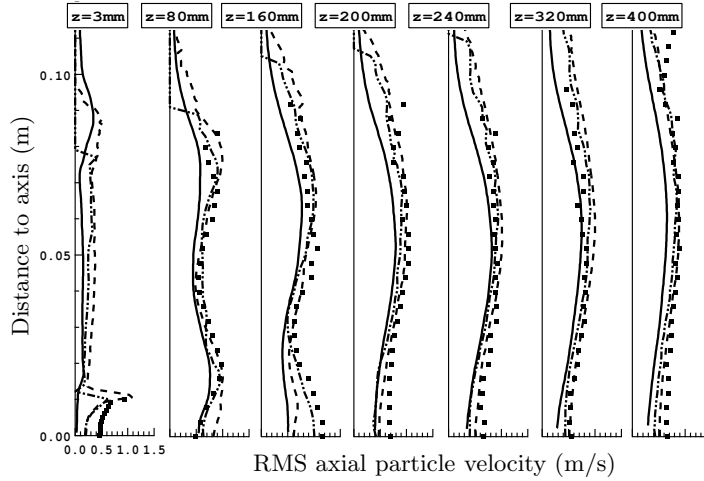


FIGURE 10. Radial profiles of RMS axial particle velocities at 7 stations along z axis. Symbols: experiment; solid line: AVBP-EE; dashed line: AVBP-EL; dot-dashed line: CDP.

of local volume fraction of solid particles for AVBP-EE on the left and CDP on the right side. Both solvers capture the zone where the solid particles accumulate. Local droplet accumulation is also observed upstream of the stagnation point within the central jet. However, the EE computation presented in Fig. 13 shows a droplet flow which stops slightly before the EL computation.

This can be quantified by plotting mean velocities along the axis for the gas (Fig. 14) and for the solid particles (Fig. 15). On this axis, the results provided by CDP are excellent while the two AVBP results match but are slightly off the experimental results. The cause of this discrepancy was investigated through various tests during the project and was identified as the absence of turbulence injected on the gas phase in the central

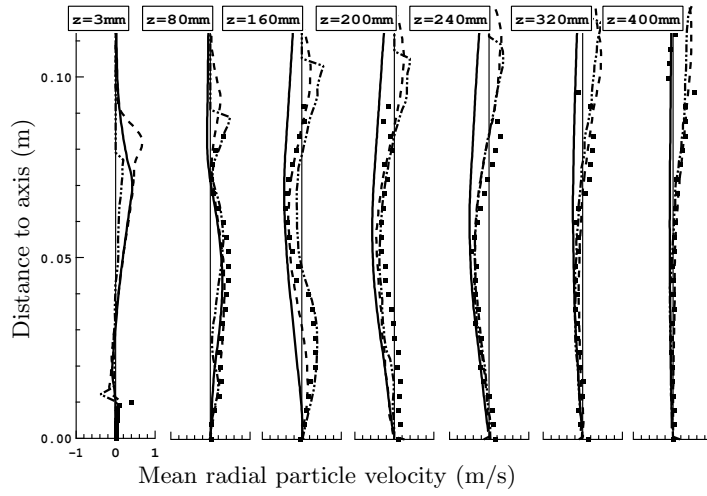


FIGURE 11. Radial profiles of mean radial particle velocities at 7 stations along z axis. Symbols: experiment; solid line: AVBP-EE; dashed line: AVBP-EL; dot-dashed line: CDP.

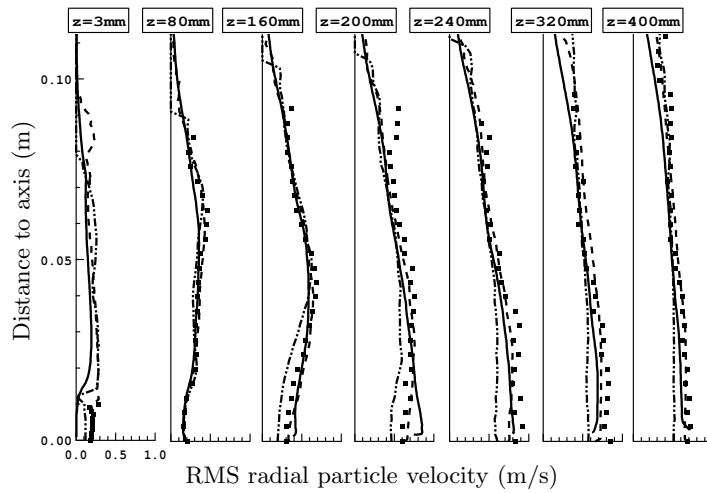


FIGURE 12. Radial profiles of RMS radial particle velocities at 7 stations along z axis. Symbols: experiment; solid line: AVBP-EE; dashed line: AVBP-EL; dot-dashed line: CDP.

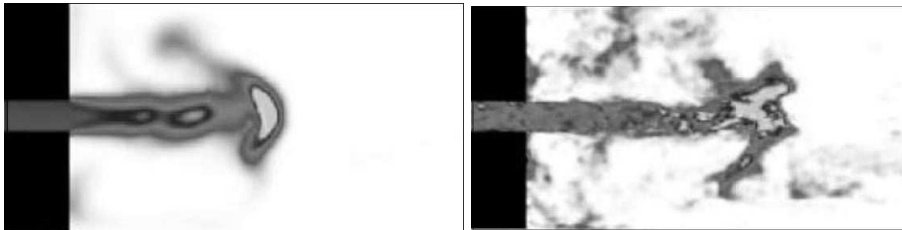


FIGURE 13. Instantaneous volume fraction in the central plane. Maximum value (black): 0.0002. Minimum value (white): 0. Right: values obtained from averaging the Lagrangian simulation in CDP. Left: output from AVBP-EE.

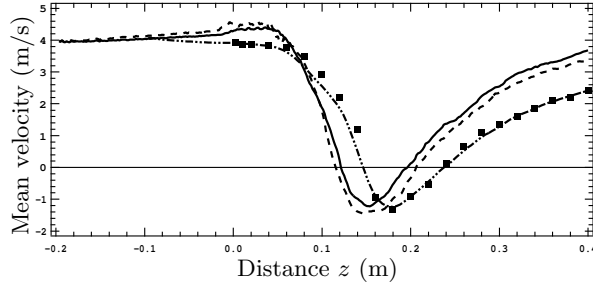


FIGURE 14. Axial profiles of mean gas velocities. Symbols: experiment; solid line: AVBP-EE; dashed line: AVBP-EL; dot-dashed line: CDP.

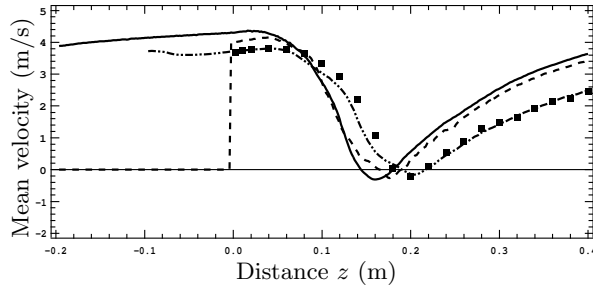


FIGURE 15. Axial profiles of mean particle velocities. Symbols: experiment; solid line: AVBP-EE; dashed line: AVBP-EL; dot-dashed line: CDP.

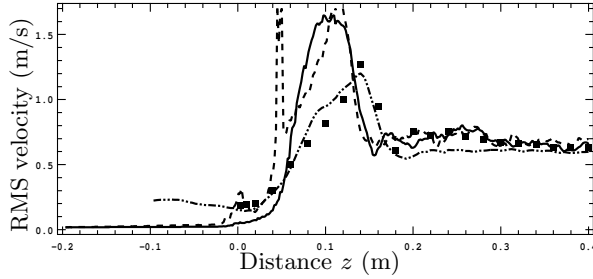


FIGURE 16. Axial profiles of RMS gas axial velocities. Symbols: experiment; solid line: AVBP-EE; dashed line: AVBP-EL; dot-dashed line: CDP.

duct in AVBP: a direct verification of this effect is that in the two AVBP computations (solid and dashed lines), the gas and the particle velocities in the central duct increase between $z = -200$ and $z = 0$ mm, indicating that the flow is relaminarizing. This also demonstrates the importance of injecting not only the proper mean profile for the gas velocity but also fluctuations with a reasonably well-defined turbulent spectrum as done in CDP. Additional tests also reveal that the injection of white noise on the particle velocities has a very limited effect on the results.

Figures 16 and 17 display axial profiles of RMS velocities for the gas and the particles. These plots confirm that the position where the maximum levels of gas and particle turbulence are found on the axis is shifted towards the jet inlet and is too intense for both AVBP computations.

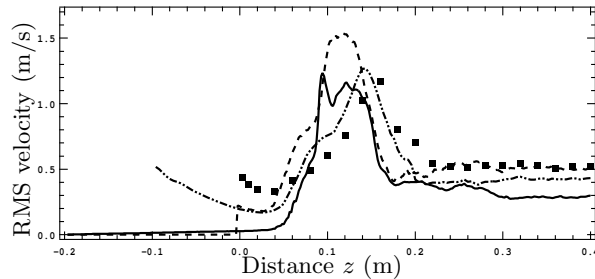


FIGURE 17. Axial profiles of RMS particle axial velocities. Symbols: experiment; solid line: AVBP-EE; dashed line: AVBP-EL; dot-dashed line: CDP.

6. Performances and conclusions

For the present test case (mass loading of 22 percent), the total number of particles present in the domain for the Lagrange codes is of the order of 600000. For such a small number of particles, the computing power required by the Lagrangian solvers compared to the power required for the gas flow remains low: the added cost due to the particles is small and no load balancing problem is observed. The EE formulation added cost (of the order of 80 percent) is independent of the mass loading so that, for the present problem, the EL formulations proved to be faster.

In terms of results quality, the EL and the EE results with AVBP are very close showing that both formulations lead to equivalent results in this situation. An important factor controlling the quality of the results is the introduction of turbulence on the gas flow in the injection duct: without these turbulent fluctuations, the results are not as good on the axis in terms of positions of the recirculation zones.

7. Acknowledgments

The help of Pr J. Borée in providing the experimental data and analyzing the results is gratefully acknowledged.

REFERENCES

- BOIVIN, M., SIMONIN, O. & SQUIRES, K. 2000 On the prediction of gas-solid flows with two-way coupling using large eddy simulation. *Phys. Fluids* **12** (8).
- BOIVIN, M., SIMONIN, O. & SQUIRES, K. 1998 Direct numerical simulation of turbulence modulation by particles in isotropic turbulence. *J. Fluid. Mech.* **375**, 235-263.
- BORÉE, J., ISHIMA, T. & FLOUR, I. 2001 The effect of mass loading and inter-particle collisions on the development of the polydispersed two-phase flow downstream of a confined bluff body. *J. Fluid Mech.* **443**, 129-165.
- CARAENI, D., BERGSTROM, C. & FUCHS, L. 2000 Modeling of liquid fuel injection, evaporation and mixing in a gas turbine burner using large eddy simulation. *Flow Turb. and Combustion* **65**, 223-244.
- CHAKRAVARTHY, V. & MENON, S. 2000 Subgrid modeling of turbulent premixed flames in the flamelet regime. *Flow Turb. and Combustion* **65**, 133-161.
- CHAPMAN, S. & COWLING, T. 1939 (digital reprint 1999) *The Mathematical Theory of*

- Non-Uniform Gases*. Cambridge Mathematical Library Edn. Cambridge University Press.
- COLIN, O., DUCROS, F., VEYNANTE, D. & POINSOT, T. 2000 A thickened flame model for large eddy simulations of turbulent premixed combustion. *Phys. Fluids* **12** (7), 1843-1863.
- COLIN, O. & RUDGYARD, M. 2000 Development of high-order Taylor-Galerkin schemes for unsteady calculations. *J. Comput. Phys.* **162** (2), 338-371.
- DRUZHININ, O.A. & ELGHOBASHI, S. 1999 On the decay rate of isotropic turbulence laden with microparticles. *Phys. Fluids* **11** (3), 602-610.
- FEDE, P., VILLEDIEU, P., SIMONIN, O. & SQUIRES, K. 2006 Stochastic modeling of the subgrid fluid velocity fluctuations seen by inertial particles. In *Proc of the Summer Program*. Center for Turbulence Research, NASA Ames/Stanford Univ.
- FÉVRIER, P., SIMONIN, O. & SQUIRES, K. 2005 Partitioning of particle velocities in gas-solid turbulent flows into a continuous field and a spatially uncorrelated random distribution: Theoretical formalism and numerical study. *J. Fluid Mech.* **533**, 1-46.
- FORKEL, H. & JANICKA, J. 2000 Large-eddy simulation of a turbulent hydrogen diffusion flame. *Flow Turb. and Combustion* **65** (2), 163-175.
- GATIGNOL, R. 1983 The Faxén formulae for a rigid particle in an unsteady non-uniform Stokes flow. *Journal de mécanique théorique et appliquée*, **1** (2), 143-160.
- GERMANO, M., PIOMELLI, U., MOIN, P. & CABOT, W. 1991 A dynamic subgrid-scale eddy viscosity model. *Phys. Fluids* **3** (7), 1760-1765.
- HAM, F. & IACCARINO, G. 2004 Energy conservation in collocated discretization schemes on unstructured meshes. In *Annual Research Briefs*, pp. 3-14. Center for Turbulence Research, NASA Ames/Stanford Univ.
- KAUFMANN, A. 2004 Vers la simulation des grandes échelles en formulation Euler/Euler des écoulements réactifs diphasiques. PhD thesis.
- KAUFMANN, A., SIMONIN, O., CUENOT, B., POINSOT, T. & HELIE, J. 2003 Dynamics and dispersion in 3D unsteady simulations of two phase flows. In *Supercomputing in Nuclear Applications*. Paris: CEA.
- KIM, J. & MOIN, P. 1985 Application of a fractional-step method to incompressible Navier-Stokes equations. *J. Comput. Phys.* **59** (2), 308-323.
- MAHESH, K., CONSTANTINESCU, G. & MOIN, P. 2004 A numerical method for large-eddy simulation in complex geometries. *J. Comput. Phys.* **197** (1), 215-240.
- MAXEY, M. & RILEY, J. 1983 Equation of motion for a small rigid sphere in a nonuniform flow. *Phys. Fluids* **26** (4).
- MOIN, P., SQUIRES, K., CABOT, W. & LEE, S. 1991 A dynamic subgrid-scale model for compressible turbulence and scalar transport. *Phys. Fluids A* **3** (11), 2746-2757.
- MOREAU, M., BÉDAT, B. & SIMONIN, O. 2005*b* A priori testing of subgrid stress models for euler-euler two-phase LES from euler-lagrange simulations of gas-particle turbulent flow. In *18th Ann. Conf. on Liquid Atomization and Spray Systems*. ILASS Americas.
- MOUREAU, V., LARTIGUE, G., SOMMERER, Y., ANGELBERGER, C., COLIN, O. & POINSOT, T. 2005 High-order methods for dns and les of compressible multicomponent reacting flows on fixed and moving grids. *J. Comput. Phys.* **202** (2), 710-736.
- PITSCH, M. & DUCHAMP DE LA GENESTE, L. 2002 Large eddy simulation of premixed turbulent combustion using a level-set approach. *Proc. of the Comb. Institute* **29**, 2001-2005.

- POINSOT, T. & VEYNANTE, D. 2005 *Theoretical and numerical combustion* R.T. Edwards, 2nd edition.
- RIBER, E., MOREAU, M., SIMONIN, O. & CUENOT, B. 2005 Towards large eddy simulations of non-homogeneous particle laden turbulent gas flows using euler-euler approach. In *11th Workshop on Two-Phase Flow Predictions*. Merseburg, Germany.
- RIBER, E., MOREAU, M., SIMONIN, O. & CUENOT, B. 2006 Development of Euler-Euler LES Approach for Gas-Particle Turbulent Jet Flow. In *Proc. Symposium Fluid-Particle Interactions in Turbulence*. 2006 ASME Joint U.S. European Fluids Engineering Summer Meeting. Miami, FEDSM2006-98110.
- ROUX, S., LARTIGUE, G., POINSOT, T., MEIER, U. & BÉRAT, C. 2005 Studies of mean and unsteady flow in a swirled combustor using experiments, acoustics analysis and large eddy simulations. *Combust. Flame* **141**, 40-54.
- SCHILLER, L. & NAUMAN, A. 1935 A drag coefficient correlation. *V.D.I. Zeitung* **77**, 318-320.
- SCHMITT, P., POINSOT, T., SCHUERMANS, B. & GEIGLE, K. 2006 Large-eddy simulation and experimental study of heat transfer, nitric oxide emissions and combustion instability in a swirled turbulent high pressure burner. *J. Fluid Mech.* **in print**.
- SELLE, L., LARTIGUE, G., POINSOT, T., KOCH, R., SCHILDMACHER, K.-U., KREBS, W., PRADE, B., KAUFMANN, P. & VEYNANTE, D. 2004 Compressible large-eddy simulation of turbulent combustion in complex geometry on unstructured meshes. *Combust. Flame* **137** (4), 489-505.
- SOMMERER, Y., GALLEY, D., POINSOT, T., DUCRUIX, S., LACAS, F. & VEYNANTE, D. 2004 Large eddy simulations and experimental study of flashback and blow-off in a lean partially premixed swirled burner. *J. of Turbulence* **5**.
- VERMOREL, O., BÉDAT, B., SIMONIN, O. & POINSOT, T. 2003 Numerical study and modelling of turbulence modulation in a particle laden slab flow. *J. of Turbulence* **4**, 025.
- VREMAN, B., GEURTS, B. & KUERTEN, H. 1995 Subgrid modeling in les of compressible flow. *Appl. Sci. Res.* **54**, 191-203.
- YOSHIZAWA, A. 1986 Statistical theory for compressible turbulent shear flows, with the application to subgrid modeling. *Phys. Fluids.* **29** (7), 2152-2164.